Inorganic Chemistry

pubs.acs.org/IC

Article

Synthesis, Structure, and Electric Conductivity of Higher Hydrides of Ytterbium at High Pressure

Tomasz Jaroń,* Jianjun Ying, Marek Tkacz, Adam Grzelak, Vitali B. Prakapenka, Viktor V. Struzhkin,* and Wojciech Grochala*

Cite This: *Inorg. Chem.* 2022, 61, 8694−8702

Read Online

ACCESS | Metrics & More | Article Recommendations | Supporting Information

ABSTRACT: While most of the rare-earth metals readily form trihydrides, due to increased stability of the filled 4f electronic shell for Yb(II), only $YbH_{2.67}$, formally corresponding to $Yb^{II}(Yb^{III}H_4)_2$ (or Yb_3H_8), remains the highest hydride of ytterbium. Utilizing the diamond anvil cell methodology and synchrotron powder X-ray diffraction, we have attempted to push this limit further *via* hydrogenation of metallic Yb and Yb_3H_8. Compression of the latter has also been investigated in a neutral pressure-transmitting medium (PTM). While the *in situ* heating of Yb facilitates the formation of YbH_{2+x} hydrides, we have not observed clear qualitative differences between the systems compressed in H_2 and He or Ne PTM. In all of these cases, a sequence of phase transitions occurred within *ca.* 13−18 GPa ($P\bar{3}1m$−$I4/m$ phase) and around 27 GPa (to the $I4/mmm$ phase). The molecular volume of the systems compressed in H_2 PTM is *ca.* 1.5% larger than of those compressed in inert gases, suggesting a small hydrogen uptake. Nevertheless, hydrogenation toward YbH_3 is incomplete, and polyhydrides do not form up to the highest pressure studied here (*ca.* 75 GPa). As pointed out by electronic transport measurements, the mixed-valence Yb_3H_8 retains its semiconducting character up to >50 GPa, although the very low remnant activation energy of conduction (<5 meV) suggests that metallization under further compression should be achievable. Finally, we provide a theoretical description of a hypothetical stoichiometric YbH_3.

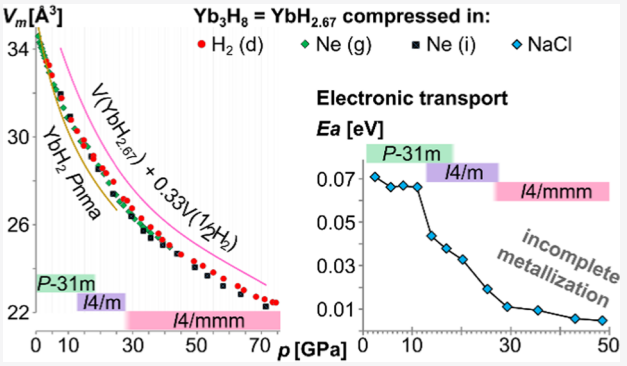

INTRODUCTION

The enormous interest in diverse hydrogen-rich systems manifested in the last few decades can be linked mainly to two topics: energy storage in chemical compounds and phonon-driven superconductivity (SC), depending on the nature of systems studied. Due to the high gravimetric efficiency required for energy storage in most potential applications, the first area has been dominated by materials composed predominantly of light elements such as Li, B, Al, etc.[1−4] On the other hand, the hydrides that have been studied as potential superconductors are not limited in this respect and their components cover virtually the entire periodic table.[5−8]

The recent upsurge in the search for high-temperature SC in hydrides under high pressure has been stimulated by Neil Ashcroft's idea of "chemical precompression" of hydrogen contained in hydrogen-rich chemical compounds.[9] In such hydrogen-dominated systems (in terms of an atomic fraction), the hydrogen sublattice is expected to contribute to the metallic state at drastically lower pressures compared to elemental hydrogen. This would finally allow for taking an advantage of the large phonon frequencies related to the lightweight hydrogen atoms to raise the critical temperature of SC. SC might occur provided the system features a high density of electronic states at the Fermi level and strong electron−phonon coupling. As a consequence of this concept, many binary and even more complex hydride-based systems have been screened theoretically,[10] leading ultimately to experimental discovery of superconductivity in some of them. Several hydrides, especially those containing the p-block and rare-earth (RE) elements,[7] were indicated as particularly promising by theoretical predictions, *e.g.*, H_3S[11,12] or YH_{10} and LaH_{10}.[13,14] The experimental verification of these predictions led to reports of strikingly high critical temperatures of superconductivity (T_C): compressed H_2S forming a superconducting H_3S phase of T_C = 203 K at 155 GPa,[15] LaH_{10} of T_C = 250−260 K upon compression to *ca.* 200 GPa,[16−18] an incompletely identified C−S−H material synthesized in a diamond anvil cell (DAC) of T_C = 288 K at

Received: February 5, 2022
Published: June 1, 2022

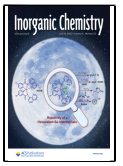

https://doi.org/10.1021/acs.inorgchem.2c00405
Inorg. Chem. 2022, 61, 8694−8702

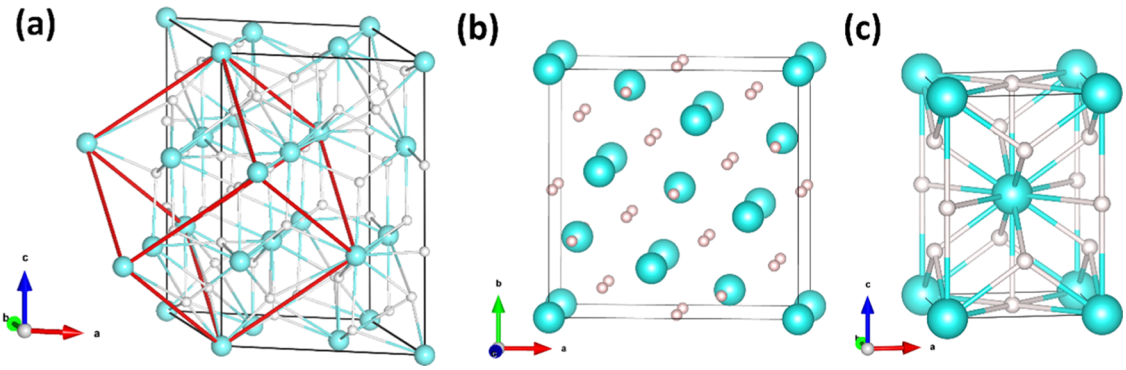

Figure 1. Overview of the crystal structures of LnH_{2+x}, Ln = Yb, Eu: (a) Yb_3H_8 ($YbH_{2.67}$) $P\bar{3}1m$;[33] (b) EuH_{2+x} $I4/m$; and (c) EuH_{2+x} $I4/mmm$.[27]

267 GPa,[19] or YH_6 of T_C = 220 K at 166−183 GPa[20,21] and YH_9 of T_C = 243−262 K at 182−201 GPa.[21,22]

Considering the RE-based systems, in these superhydrides, the hydrogen sublattice is usually composed of clathrate-like and other complex geometrical motifs or contains mixed molecular and atomic units.[5,10,23] While the polyhydrides of exotic compositions may form in a megabar pressure range, they are preceded by more usual stoichiometries appearing at much lower pressures. Some of the latter also superconduct, as has been verified experimentally or as expected based on computational screening.[7] Obviously, lowering the pressure of synthesis of a superconducting hydride or the metastability of such phases under as close to ambient conditions as possible would be beneficial for more thorough macroscopic studies and possible applications. Recently, such high-temperature superconducting phases have been found for the hydrides based on lanthanides below the megabar pressure region.[24,25]

With the exception of Eu and Yb, all lanthanides are easily hydrogenated at room temperature, absorbing up to 300 mol % hydrogen to form trihydrides, LnH_3, already under the pressure of a few atmospheres;[26] see also Figure S1 in the Supporting Information (SI). However, due to the stabilization of half-filled or filled 4f electronic shells for Eu(II) and Yb(II), respectively, oxidation of these elements to the trivalent state by hydrogen is much more difficult. While the corresponding dihydrides can be readily prepared,[26] further absorption of hydrogen requires significantly higher pressure. The uptake of hydrogen by EuH_2 occurs only above 8.7 GPa, as has been reported by Matsuoka et al. based on X-ray diffraction and Eu−Mössbauer spectroscopy measurements.[27] At this pressure range, a tetragonal EuH_{2+x} containing trivalent Eu^{3+} starts to form, and the latter remains the only detected oxidation state of Eu above 12.5 GPa.[28] Very recently, Semenok et al.[29] reported that EuH_9 is present in the samples already at 74 GPa, while the other europium superhydrides were detected within the range 74−130 GPa, some of them showing antiferromagnetic ordering. Unfortunately, the lower-pressure regime has not been studied in this work, leaving the gap between *ca.* 50 GPa for which EuH_{2+x} phases were reported and 74 GPa with the superhydride phases already formed.

In the case of ytterbium, some early reports indicated preparation of cubic YbH_{2+x}, $x < 0.7$ after reaction of this metal with hydrogen pressurized to *ca.* 120 bar.[30−32] These findings have been clarified by Auffermann, who prepared the metastable higher hydride of ytterbium *via* a high-pressure, high-temperature reaction (200−3200 bar, >600 K).[33] While the major features of the powder X-ray diffraction pattern of YbH_{2+x} are compatible with a face-centered cubic (fcc) unit cell reported earlier, application of powder neutron diffraction allowed for proper identification and refinement of its crystal structure. It appeared that the prepared compound can be described as $YbH_{2.67}$, *i.e.*, Yb_3H_8 or $Yb^{II}(Yb^{III}H_4)_2$, and it crystallizes in a trigonal unit cell with close packing of the nine ytterbium atoms (stacking sequence: ...ABC...), while hydrogen occupies all of the tetrahedral and 2/3 of the octahedral holes, and no disorder is observed in the structure. The crystal structures of the higher hydrides of Yb and Eu relevant to the current study are summarized in Figure 1.

The case of Yb(III) is special.[2] The vicinity of 4f shell closure for the $4f^{13}$ electron configuration of Yb^{III} resembles the $3d^9$ configuration of parent oxocuprate superconductors, and the early DFT calculations indicated the possibility of the significant contribution of H 1s states to the electron density at the Fermi level even for the stoichiometric Yb(III) hydrides.[34] Markedly, the only hole in the f electron set usually resides on the orbital, which forms sigma* states with H(1s), which is analogous to a hole in the d set of Cu(II) residing in sigma* states with O(2p) in cuprates. Moreover, Yb(III) features a large magnetic moment of *ca.* 4.3−4.9 m_B corresponding formally to spin-1/2, which again renders it similar to Cu(II) in parent compounds of oxocuprate superconductors; thus, one might expect that electron doping could affect magnetism and lead to SC, just like for Cu(II) oxides. Last but not the least, more recent theoretical considerations suggest that besides yttrium and the lightweight lanthanides (Ln),[13,14,35] the late lanthanides (Yb and Lu) should also form the superhydrides of T_C > 100 K.[36]

In the present work, we expand the chemistry of the Yb−H system far beyond the previously studied range of *ca.* 0.3 GPa. Using the DAC methodology, we investigate the reaction of metallic Yb with H_2 and attempt further hydrogenation of Yb_3H_8 ($YbH_{2.67}$). We discuss the observed phase transitions as well as the possibility of formation of the higher hydrides of ytterbium, *i.e.*, YbH_{2+x}, especially with x > 0.67. We have also studied the electronic transport of the mixed-valence Yb_3H_8 in the function of external pressure.[37]

METHODS

Experimental Section. Metallic Yb (99.9%, Sigma-Aldrich) and Au pressure standard (99.999%, Alfa Aesar) were loaded into the DAC. Diamonds of 200−300 μm culets and rhenium gaskets were used. Yb_3H_8 was prepared according to the literature procedure[33] and analyzed at ambient conditions using powder X-ray diffraction, *cf.* Figure S2 and Table S1 in the SI. Ne, He, and H_2, loaded at *ca.* 170 MPa in the custom-designed gas loading systems of GL CIW and

https://doi.org/10.1021/acs.inorgchem.2c00405
Inorg. Chem. 2022, 61, 8694−8702

Table 1. Selected Low-Angle Reflections Originating from the Distinct Phases, as Marked in Figure 2−4 and Their Lattice Parameters[a]

phase	lattice parameters	reflections
YbH_{2+x} $P\bar{3}1m$	4.9 GPa: a = 6.21623(13) Å, c = 8.8237(5) Å	a_1-(1 0 0), a_2-(1 0 1), a_3-(0 0 3), and (2 $\bar{1}$ 1), a_4-(1 1 2), a_5-(2 $\bar{1}$ 4), and (3 0 0)
YbH_{2+x} $I4/m$	20.6 GPa: a = 7.6386(2) Å, c = 4.8978(3) Å	b_1-(1 0 1), b_2-(2 0 0), b_3-(2 1 1), b_4-(0 0 2), and (3 1 0), b_5-(3 1 2) and (4 2 0)
YbH_{2+x} $I4/mmm$	39.2 GPa: a = 3.2837(8) Å, c = 4.6955(11) Å	c_1-(1 0 1), c_2-(0 0 2), and (1 1 0), c_3-(1 1 2) and (2 0 0), c_4-(1 0 3) and (2 1 1)
YbH_2 $Pnma$	3.6 GPa: a = 5.7134(3) Å, b = 3.49242(15) Å, c = 6.6346(4) Å	h_1-(1 0 1), h_2-(0 0 2), h_3-(0 1 1), h_4-(1 0 2), and (2 0 0), h_5-(1 1 1)
Yb $Fm\bar{3}m$	3.6 GPa: a = 5.1173(4) Å	y_1-(1 1 1), y_2-(0 0 2)

[a]For more specific data, see the Supporting information.

GSE CARS APS,[38] were applied as the pressure-transmitting medium (PTM).

High-pressure angle-dispersive X-ray diffraction (XRD) measurements were performed using the Advanced Photon Source synchrotron facility of the Argonne National Laboratory. The measurements were carried out on sectors 13ID-D and 16ID-B operating at wavelengths from 0.2952 to 0.4066 Å. The sample-to-detector distance and other geometrical parameters were calibrated using LaB_6 or CeO_2 standards. One of the samples of Yb in H_2 PTM was heated by the double-sided laser systems available at the beamlines to the maximum temperatures of about 2100 K measured by fitting gray body thermal radiation.[39] Heating was carried out in several pulses lasting for a few seconds; however, the overall amount of energy absorbed by the sample was not monitored. The heating was not uniform across the sample, which manifested as variable amounts of crystalline phases present in various areas of the sample.

The electronic transport properties were carried out in a custom, miniaturized diamond anvil cell in a classical four-electrode geometry, using a Quantum Design Physical Property Measurement System. NaCl was used as a PTM, and the pressure was measured using ruby fluorescence.

The two-dimensional diffraction images were analyzed and integrated using DIOPTAS software.[40] X-cell was used for pattern indexing.[41] The structures were refined in JANA2006.[42] The pseudo-Voigt function with the Berar−Baldinozzi correction for asymmetry was utilized for modeling the diffraction peak shape. The background was corrected by Legendre polynomials. Further details of the crystal structure investigations may be obtained from the joint CCDC/FIZ Karlsruhe online deposition service: https://www.ccdc.cam.ac.uk/structures/ by quoting the deposition numbers CSD 2150168−2150171. The third-order Birch−Murnaghan equations of state (EoS) were fitted using the EoSFit7-GUI program.[43,44]

Computational. Density functional theory (DFT) calculations were performed using CASTEP.[45] Generalized gradient approximation (GGA) was used with the PBE functional adjusted for solids (PBEsol).[46] As hydrides usually require a large cutoff, here the value of 700 eV was applied to lead to very good energy convergence. The density of the k-point grid was set at 0.04 $Å^{-1}$; ultrasoft pseudopotentials generated on the fly were used as they provide more accurate lattice parameters. The YbH_3 stoichiometry was assumed, and the $I4/mmm$ structure type exhibited by YbH_{2+x} at elevated pressures was adopted. The sqrt2 × sqrt2 × 1 supercell (Z = 4) was applied to account for various magnetic ordering schemes; the formal spin of Yb(III) was used as the initial one in the first SCF step. For the magnetic structures, the DFT + U formalism was used, with U = 5 eV for the 4f electrons of Yb. Enthalpies of various magnetic models and that of a spin-unpolarized one were calculated at several pressure values. Electronic density of states (DOS) was computed for the lowest enthalpy solutions.

RESULTS AND DISCUSSION

As could be expected, the reaction between metallic ytterbium and hydrogen proceeds already at room temperature immediately after hydrogen loading to the cell. However, the unreacted metal is present in the whole pressure range studied, contributing to the strongest diffraction peaks (*cf.* Table 1), even for the largest pressure achieved for the sample compressed at room temperature to *ca.* 40 GPa; see Figures S3−S4. The evolution of the crystalline phases detected in this sample well corresponds to that described earlier, and YbH_2 remains the main hydridic phase.[47−49] The crystalline phase, which can be attributed to a higher hydride of ytterbium, YbH_{2+x}, is barely detected even at *ca.* 40 GPa; see Figure S3. However, the composition is variable from sample to sample, and in the case of the second DAC, the clear, although relatively weak, signals of the $P\bar{3}1m$ phase of YbH_{2+x} are visible already at 3.6 GPa, before heating of the sample; see Figure 2a. This may be attributed to a variable degree of surface oxidation, which should hamper further hydrogenation of the sample (this problem has been recently addressed using a thin Pd coating for the synthesis of yttrium superhydrides).[22]

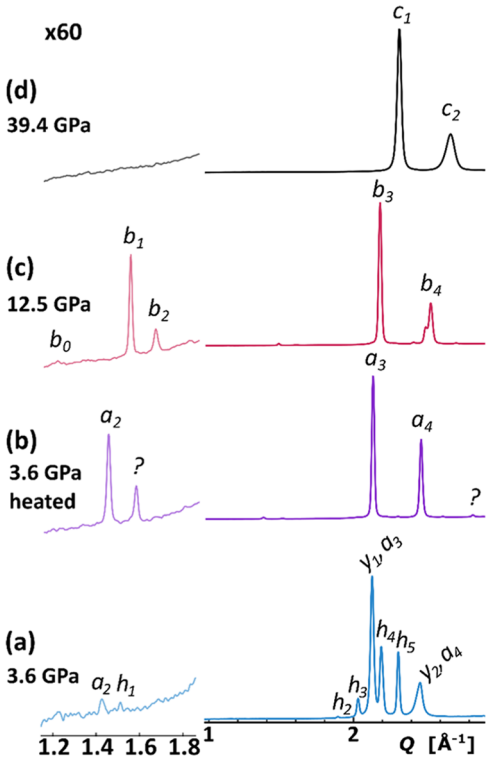

Figure 2. Diffraction patterns for the sample of Yb compressed in H_2: (a) before and (b) after the laser heating at *ca.* 3.6 GPa; (c) after several rounds of laser heating (*ca.* 12.5 GPa); and (d) at *ca.* 39.4 GPa. The low-Q part has been additionally presented in 60× magnification of intensity. λ = 0.3344 Å. a-YbH_{2+x} $P\bar{3}1m$: 2-(1 0 1), 3-(0 0 3), and (2 $\bar{1}$ 1), 4-(1 1 2); b-YbH_{2+x} $I4/m$: 0-(1 1 0), 1-(1 0 1), 2-(2 0 0), 3-(2 1 1), 4-(0 0 2), and (3 1 0); c-YbH_{2+x} $I4/mmm$: 1-(1 0 1), 2-(1 1 0), and (0 0 2); h-YbH_2 $Pnma$: 1-($\bar{1}$ 0 1), 2-(0 0 2), 3-(0 1 1), 4-(1 0 2), and (2 0 0), 5-(1 1 1); y-Yb $Fm\bar{3}m$: 1-(1 1 1), 2-(0 0 2).

https://doi.org/10.1021/acs.inorgchem.2c00405
Inorg. Chem. 2022, 61, 8694−8702

The *in situ* laser heating of the partially hydrogenated ytterbium sample up to *ca.* 2100 K, with several pulses lasting for a few seconds each, facilitates further hydrogenation and delivers the $P\bar{3}1m$ phase of YbH_{2+x} (Figure 1a), which predominates the powder diffraction pattern; see Figures 2b and S5−S7. The YbH_2 is detected in the sample in a minor amount, together with very weak signals from an unidentified crystalline phase(s); see Figure S7. Although the sample does remain not fully homogeneous, it can be concluded that both of these phases disappear after a few additional heating cycles on larger compression; see Figure S8. Above *ca.* 12.5 GPa, the $P\bar{3}1m$ phase of YbH_{2+x} undergoes a transition to the $I4/m$ phase, which is isostructural to that reported for EuH_{2+x} at 8.7−9.7 GPa,[27] as indicated by the peak splitting (*e.g.*, the peak b_4 of (0 0 2) and (3 1 0) reflections, while the (1 1 2) reflection of the trigonal phase contributes solely to the related a_4 peak) and the low-intensity reflections from the tetragonal superstructure (*e.g.*, (1 1 0), (1 0 1), and (2 0 0), marked as b_0, b_1, and b_2, respectively); see Figure 2c. During further compression, the latter phase symmetrizes to the $I4/mmm$ structure (Figure 2d), similar to the EuH_{2+x} analogue reported for hydrogen pressures exceeding 9.7 GPa.[27] That second phase transition manifests itself as the vanishing superstructure signal and as a less-pronounced peak splitting for the main peaks (*e.g.*, c_2 corresponding to (0 0 2) and (1 1 0) reflections).

To deal with more homogeneous samples including those with a fixed content of hydrogen, we also investigated Yb_3H_8 (YbH_{2+x}, x = 0.67), which was prepared *ex situ* according to Auffermann's procedure;[33] here, Yb_3H_8 was studied in DAC under compression in H_2 or in He or Ne pressure-transmitting media (PTM). The evolution of the crystalline phases for Yb_3H_8 compressed in H_2 or an inert PTM well corresponds to that observed for the sample of ytterbium heated in H_2; see Figures 3 and S10−S23. It appears that the $P\bar{3}1m$ and $I4/m$ phases coexist within the range of *ca.* 13−18 GPa regardless of the PTM. The superstructure signals of the $I4/m$ phase vanish above *ca.* 27 GPa, indicating the transition to the $I4/mmm$ phase. However, minor low-angle diffraction peaks were still observed for some of the Yb_3H_8 samples compressed in the neutral PTM above 35 GPa (Figure S20). The high-symmetry $I4/mmm$ phase of YbH_{2+x} remains stable up to the highest pressures reached in our investigations of *ca.* 75 GPa; see Figure 3. The first phase transition ($P\bar{3}1m \rightarrow I4/m$) occurs with significant changes in the first coordinating spheres and is sluggish, as both phases are detected within the *ca.* 5 GPa range (this resembles the behavior of YbH_2).[49] These observations suggest a reconstructive phase transition, possibly of the first-order despite no significant volume discontinuity being observed. The second phase transition ($I4/m \rightarrow I4/mmm$) does not require significant changes in the coordination spheres but is rather related to symmetrization of the atomic positions. Therefore, it is a displacive phase transition apparently of the second order.

The transition pressure between the $I4/m$ and $I4/mmm$ phases of YbH_{2+x} is markedly higher than that of EuH_{2+x} containing larger metal ions.[27] This trend remains in line with the known relations observed for the Ln^{3+} compounds, *e.g.*, following the row of contracting Ln^{3+} ions, the hexagonal-to-cubic transition in the LnH_3 series gradually requires a higher pressure,[50,51] and a similar trend was noticed for the phase transitions of Ln_2O_3.[52] Clearly, the smaller cations require higher compression to mimic the larger ones, which is a common trend in high-pressure chemistry.[53]

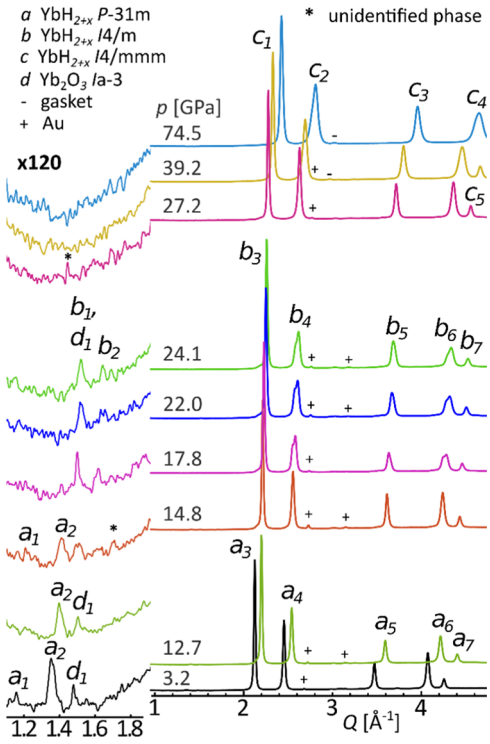

Figure 3. Diffraction patterns for the sample of Yb_3H_8 compressed in H_2 at room temperature. The low-Q part has been additionally presented in 120× magnification of intensity. λ = 0.4066 Å. a-YbH_{2+x} $P\bar{3}1m$: 1-(1 0 0), 2-(1 0 1), 3-(0 0 3), and (2 -1 1), 4-(1 1 2); b-YbH_{2+x} $I4/m$: 1-(1 0 1), 2-(2 0 0), 3-(2 1 1), 4-(0 0 2), and (3 1 0); c-YbH_{2+x} $I4/mmm$: 1-(1 0 1), 2-(1 1 0), and (0 0 2).

The diffraction patterns from Yb_3H_8 samples in H_2 and Ar PTMs (Figure 4) are quite similar to each other. All key reflections may be assigned to the same crystalline phase in both data sets. Such a qualitative picture alone may suggest that an additional H_2 uptake does not occur for Yb_3H_8 even at 74.5 GPa, the highest pressure reached in our experiments. However, for the $I4/mmm$ phase, the corresponding diffraction signals are shifted toward lower Q values for the sample of Yb_3H_8 compressed in H_2 PTM, indicating a larger unit cell volume. This phenomenon is noticeable around 30 GPa, becoming obvious for larger pressures (Figure S23).

EoS for Yb_3H_8 was derived independently for the YbH_{2+x} crystalline phases present in the samples compressed in H_2 and Ne PTMs for the experimental runs covering a sufficient number of $V(p)$ data points; see Figures S24−S29. The obtained fit parameters are presented in Table 2, while some of the available EoS parameters for the related lanthanide hydrides are summarized in Table S2. In general, the V_0 of the low-pressure trigonal form is slightly larger than the high-pressure $I4/mmm$ phase, and the inverse trend is observed for their bulk moduli. The $P\bar{3}1m$ form of Yb_3H_8 reveals V_0 comparable to the *Pnma* YbH_2 of V_0 = 35.63(7) Å^3, but the former remains significantly less compressible (Figure 5) (for *Pnma* YbH_2 B_0 = 40.2(22) GPa).[48] The $I4/mmm$ phase of YbH_{2+x} present above *ca.* 27 GPa has a slightly smaller molecular volume with an increased bulk modulus. These values fulfill a similar trend for the europium hydrides: the $I4/mmm$ phase of EuH_{2+x} of V_0 = 38.8(1) Å^3 (slightly bulkier than the Yb analogue, according to the relation of Eu and Yb ionic

https://doi.org/10.1021/acs.inorgchem.2c00405
Inorg. Chem. 2022, 61, 8694−8702

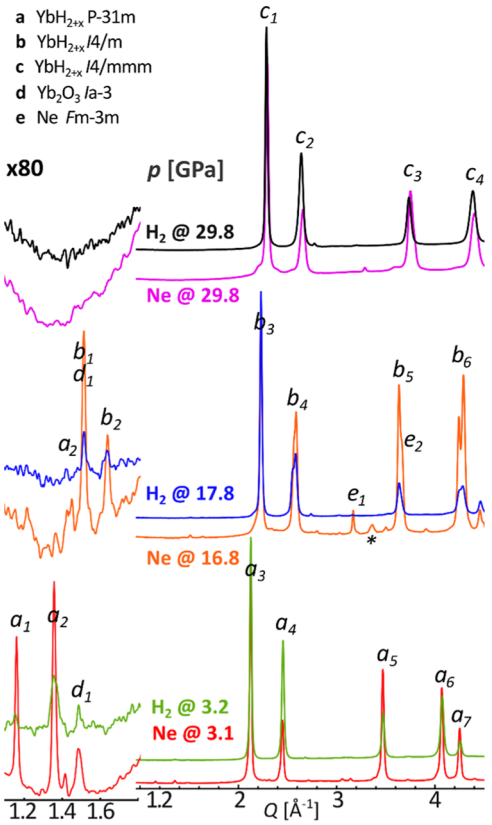

Figure 4. Comparison of the integrated diffraction data for Yb_3H_8 compressed in Ne and in H_2. The low-Q region has been expanded (left). λ = 0.3344 Å (Ne at 3.1 and 16.8 GPa), 0.2952 Å (Ne at 29.8 GPa), and 0.4066 Å (H_2). The most visible reflections of the YbH_{2+x} and Yb_2O_3 phases were marked: a-YbH_{2+x} $P\bar{3}1m$: 1-(1 0 0), 2-(1 0 1), 3-(0 0 3), and (2 $\bar{1}$ 1), 4-(1 1 2); b-YbH_{2+x} $I4/m$: 1-(1 0 1), 2-(2 0 0), 3-(2 1 1), 4-(0 0 2), and (3 1 0); c-YbH_{2+x} $I4/mmm$: 1-(1 0 1), 2-(0 0 2), and (1 1 0), 3-(1 1 2), and (2 0 0), 4-(1 0 3), and (2 1 1). * indicates the strongest signal from the unidentified phase.

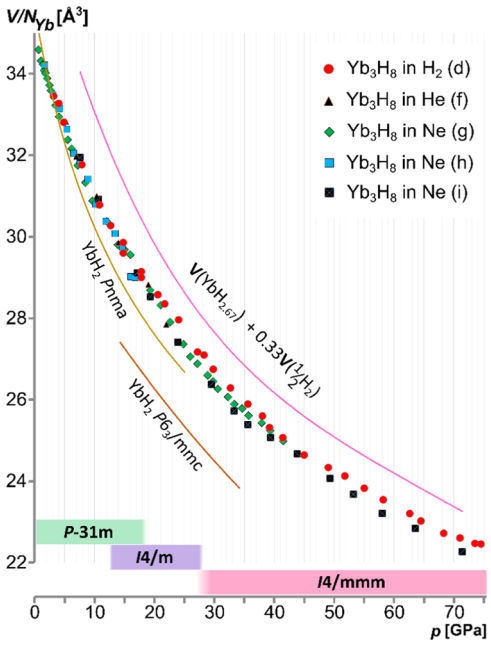

Figure 5. Volume per ytterbium atom in the function of pressure for the compression of Yb_3H_8 in H_2, He, and Ne at room temperature. The molecular volume of YbH_2[48] and the volume roughly estimated for YbH_3 have also been plotted. The crystallographic phases of YbH_{2+x}, detected under a specific pressure range, are indicated at the bottom. Notice that the sample (d) represents a system of variable stoichiometry due to gradual H_2 uptake.

radii) shows a significantly higher bulk modulus in comparison to the dihydride (B_0 = 69(2) GPa *vs* B_0 = 40−45 GPa for the two polymorphs of EuH_2).[54] Contrastingly, the trihydrides of the neighboring lanthanides (especially the Sm for Eu and Er or Tm for Yb) reveal rather larger values of the bulk moduli, while the V_0 of the *I*4/*mmm* forms of EuH_{2+x} and YbH_{2+x} falls close to the values reported for hexagonal and cubic polymorphs of the respective LnH_3, Ln = Sm (for Eu), Er, and Tm (for Yb); see Table S2.

One key issue is that of the composition of the YbH_{2+x} specimen studied and that of a possible H_2 uptake by the sample in the H_2 atmosphere. Inspection of Figure 5 reveals that the differences in the molar volume of the Yb_3H_8 specimen compressed in various PTMs are only marginal, which is also reflected by the respective EoS curves; see Figure S30. However, on larger compression, the $V(p)$ curve seems to be slightly less steep for the sample pressurized in H_2. Although the discrepancy is rather small and it may be caused by the errors in the determination of pressure in both types of samples, it is fairly consistent across the pressures for which the tetragonal phases are favored, especially 25−75 GPa. The EoS curves fitted for the *I*4/*mmm* YbH_{2+x} in H_2 and Ne PTM fall apart by *ca.* 1.5% in terms of $V(p)$; see Figure S31. At the same time, a simple addition of 1/3 atomic volume of hydrogen would increase the molecular volume of *I*4/*mmm* YbH_{2+x} by *ca.* 4.8% at this pressure range. Altogether, this might suggest that the composition of the sample compressed in excess H_2 is similar to $YbH_{2.77}$ rather than $YbH_{2.67}$.

Indeed, one might speculate that the amount of 1/3 of vacancies is not a natural value for the tetragonal *I*4/*mmm* cell and that 1/4 would be a more natural value (hence, $YbH_{2.75}$ would be a more appropriate composition for such a specimen,

Table 2. Summary of the Parameters of the Third-Order Birch−Murnaghan EoS Obtained from the Compression Data[a]

phase of YbH_{2+x}	PTM, sample	V_0 per Yb atom [Å^3]	B_0 [GPa]	B_0'	max Δp [GPa]	x^2, N
$P\bar{3}1m$	Ne, (g)	35.033(32)	56.13(63)	5.5	0.31	1.82, 19
	Ne, (h)	35.31(12)	53.4(19)	5.5	−0.43	6.82, 11
	H_2, (d)	35.292(88)	55.0(14)	5.5	0.22	3.26, 8
*I*4/*m*	Ne, (g)	35.82(23)	63.1(22)	3.0	−0.31	1.15, 8
*I*4/*mmm*	Ne, (i)	34.05(34)	64.0(33)	4.5	1.03	7.95, 10
	H_2, (d)	34.98(27)	59.7(23)	4.5	1.67	7.21, 19

[a]The estimated standard deviations (E.S.Ds.) are given in parentheses. B_0' was fixed for the final refinement. N represents the number of data points.

https://doi.org/10.1021/acs.inorgchem.2c00405
Inorg. Chem. 2022, 61, 8694−8702

very close to $YbH_{2.77}$ suggested above from the EOS analyses). However, due to lack of direct evidence supporting such a scenario, one must refrain from making any firm conclusions here. In any case, the stoichiometry of the samples studied must be still far from the one expected for the Yb(III)H_3 stoichiometry (Figure 5, n.b. the V/N_{Yb} curve of YbH_3 may only serve as a rough estimation as the effects of the strain introduced during crystal formation were not considered). Resistance of Yb to be fully oxidized to Yb(III) in the hydride environment is remarkable; it turns out that only if a negative charge density on the hydride is reduced, *e.g.*, by binding it to B(III) in the form of the BH_4^- anion, the stoichiometric Yb(III) species may form and yet they are thermodynamically metastable at ambient (p,T) conditions.[55−58]

The electric conductivity of formally mixed-valence species, be it $YbH_{2.67}$, $YbH_{2.75}$, or $YbH_{2.77}$, is of great interest in the context of potential generation of superconductivity in this material. Figure 6 (top) shows the electric resistivity versus

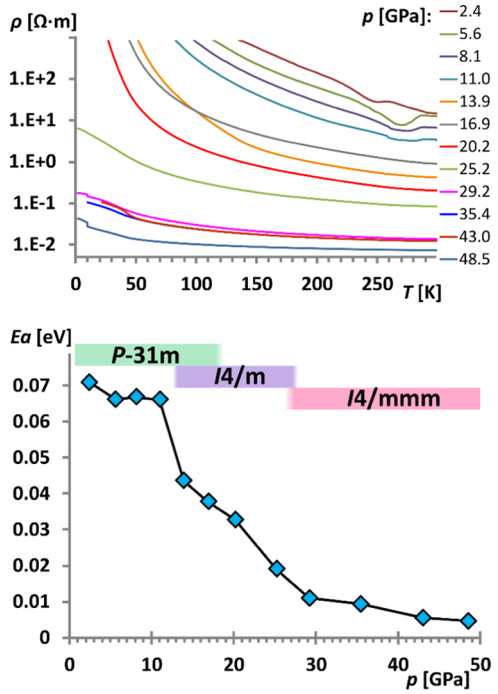

Figure 6. Resistivity *vs* T[K] for Yb_3H_8 compressed in NaCl presented in a logarithmic scale indicating a semiconductor-like behavior (top). Evolution of the activation energy of the electronic transport as a function of pressure (bottom). Despite the significant decrease of E_a, the system avoids full metallization until 50 GPa (the highest pressure in our experiment).

temperature plot for a sample of Yb_3H_8 embedded in NaCl PTM. It is clear that the low-pressure phases of Yb_3H_8 show a semiconducting behavior as their resistivity strongly decreases with the temperature increasing. A large drop in resistivity may be seen between 20.2 and 25.2 GPa, roughly corresponding to the second structural phase transition from the $I4/m$ to the $I4/mmm$ polymorphs.

Analysis of the activation energy for conductivity, E_a (Figure 6 bottom), suggests that E_a is already quite small (*ca.* 0.07 eV or 812 K) for Yb_3H_8 at a low pressure (2.4 GPa). This feature comes certainly from the mixed-valence nature of the compound. One sharp drop of the E_a value is seen between 11.0 and 13.9 GPa, roughly corresponding to the first crystallographic phase transition. The second drop of the E_a value between 20 and 29 GPa is more subtle, which suggests that the second phase transition affects E_a less considerably, and it is followed by the flattening of the curve above *ca.* 29 GPa. The E_a value determined at 48.5 GPa is as small as 0.005 eV (58 K) yet not null. Thus, Yb_3H_8 retains its semiconducting character even at *ca.* 50 GPa; this makes it similar to Fe_3O_4.[59] Metallicity, which would correspond to the formulation of Yb(III)$_3H_8(e^-)$, might be within the reach of the 1 Mbar experiments.

To learn what properties might be expected from fully stoichiometric YbH_3, we performed quantum mechanical calculations for this compound; we assumed that it would adopt the $I4/mmm$ structure observed here, similar to the europium analogue for which solely the Eu^{3+} oxidation state has been detected above 12.5 GPa.[28] Both the magnetic and spin-unpolarized models were considered. The molecular volumes calculated for these models of YbH_3 fall within the range of experimentally observed values for the $YbH_{2.67}$ and $YbH_{2.67+x}$ compounds (Figure S33), which may indicate a slight underestimation of the lattice parameters by the applied DFT formalism. At the same time, the molecular volume computed for the YbH_4 polyhydride ($I4/mmm$, isostructural with the proposed YH_4 and other REH_4)[60] remains significantly larger.

The DFT calculations for all magnetic states converge to solutions characterized by extremely small remnant magnetic moments. The corresponding spin-nonpolarized band structure and DOS (Figure 7) suggest that the compound would have a metallic nature, with several broad bands crossing the Fermi level. Both Yb(f) and H(s) states contribute to the states at the Fermi level; such strong hybridization was noticed previously.[34] The fact that the spin of Yb(III) would not localize but instead give rise to itinerant electrons may seem surprising, but this could be due to strong hybridization with broad H(s) states (and this was the reason why we were targeting YbH_3 composition in experiments).

CONCLUSIONS

We have attempted synthesis of the yet-elusive ytterbium trihydride utilizing both metallic Yb and its currently most hydrogen-rich hydride, $YbH_{2.67}$, as the precursors in high-pressure hydrogenation (up to *ca.* 75 GPa). Our results point to the lack of a marked qualitative difference between these systems compressed in H_2 and the samples of $YbH_{2.67}$ pressurized in He or Ne PTM. In all of these cases, a sequence of phase transitions from the unit cells of the $P\bar{3}1m$ symmetry to the $I4/m$ and $I4/mmm$ systems occurred within *ca.* 13−18 GPa and around 27 GPa, respectively. The same tetragonal phases were observed upon compression of EuH_2 in H_2 PTM: the $I4/m$ Eu^{2+}/Eu^{3+} mixed-valence system formed from the $P6_3/mmc$ dihydride above 8.7 GPa and the high-symmetry $I4/mmm$ phase was detected above 9.7 GPa.[27] The fact that Eu^{3+} in a hydride environment forms at a pressure as large as 8.7 GPa, while analogous species of Yb^{3+} may be prepared at several kPa, is following the standard redox potentials of the Eu^{3+}/Eu^{2+} and Yb^{3+}/Yb^{2+} pairs, which are −0.35 and −1.05 V, respectively. In other words, Yb^{2+} can be easier oxidized by H_2 to Yb^{3+} than its Eu^{2+} analogue.

For the highest pressure investigated here (25−75 GPa) corresponding to the $I4/mmm$ phase, the molecular volume of the systems compressed in H_2 PTM consistently remains *ca.* 1.5% larger than that for the systems compressed in inert gas

https://doi.org/10.1021/acs.inorgchem.2c00405
Inorg. Chem. 2022, 61, 8694−8702

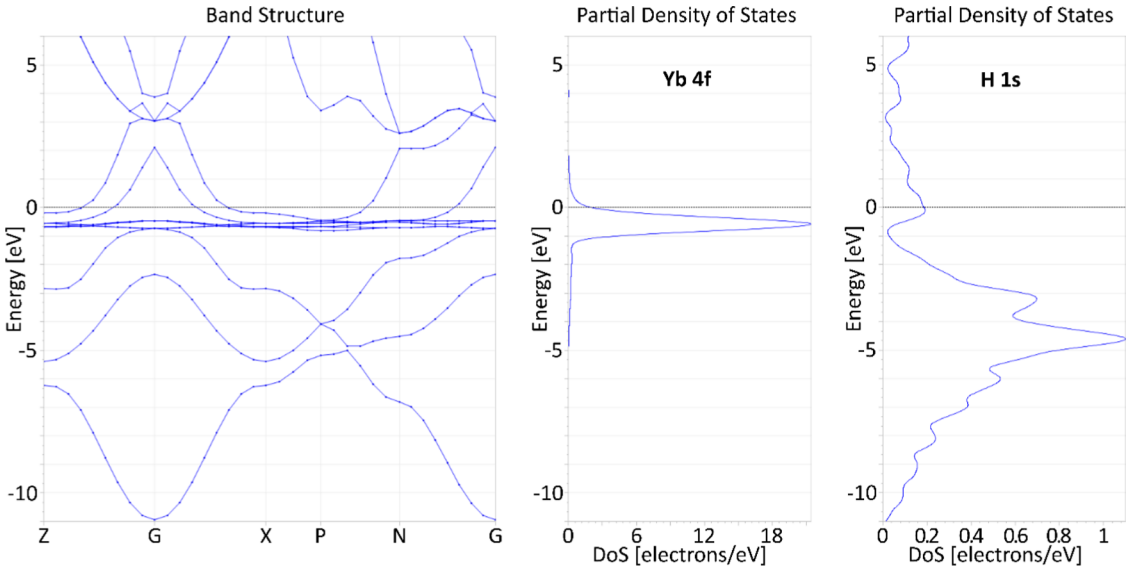

Figure 7. Electronic band structure (left) and DOS (Yb 4f center, H 1s right) for the spin-unpolarized solution, for YbH_3 in the *I*4/*mmm* structure type at 50 GPa. Note the partial DOS scale difference between those for Yb and H electrons.

media. Such a difference in the molecular volume indicates incremental hydrogenation with the possible formation of $YbH_{2.75-2.77}$ at *ca.* 75 GPa. However, additional research is necessary to fully identify the stoichiometry achieved upon hydrogenation, and an even rather larger pressure is needed to push the system toward stoichiometric YbH_3 or ytterbium polyhydrides. Such compounds should be interesting due to their metallic nature, as expected on the basis of DFT calculations for YbH_3. At the same time, while the mixed-valence Yb_3H_8 retains its semiconducting character up to at least 50 GPa, the very low remnant activation energy of conduction (<5 meV) suggests that the metallization under further compression of this mixed-valence compound should also be achievable.

■ ASSOCIATED CONTENT

Supporting Information

The Supporting Information is available free of charge at https://pubs.acs.org/doi/10.1021/acs.inorgchem.2c00405.

Raw experimental data, additional figures and plots, profile and structure refinement results; CIF files—full structural details (PDF)

Accession Codes

CCDC 2150168−2150171 contain the supplementary crystallographic data for this paper. These data can be obtained free of charge via www.ccdc.cam.ac.uk/data_request/cif, or by emailing data_request@ccdc.cam.ac.uk, or by contacting The Cambridge Crystallographic Data Centre, 12 Union Road, Cambridge CB2 1EZ, UK; fax: +44 1223 336033.

■ AUTHOR INFORMATION

Corresponding Authors

Tomasz Jaroń − *Centre of New Technologies, University of Warsaw, 02-097 Warsaw, Poland; Geophysical Laboratory, Carnegie Institution of Washington, Washington, District of Columbia 20015, United States; Faculty of Chemistry, University of Warsaw, 02-089 Warsaw, Poland;* orcid.org/0000-0002-5514-6133; Email: tjaron@uw.edu.pl

Viktor V. Struzhkin − *Geophysical Laboratory, Carnegie Institution of Washington, Washington, District of Columbia 20015, United States; Center for High Pressure Science and Technology Advanced Research, Shanghai 201203, China;* Email: viktor.struzhkin@hpstar.ac.cn

Wojciech Grochala − *Centre of New Technologies, University of Warsaw, 02-097 Warsaw, Poland;* orcid.org/0000-0001-7317-5547; Email: w.grochala@cent.uw.edu.pl

Authors

Jianjun Ying − *Geophysical Laboratory, Carnegie Institution of Washington, Washington, District of Columbia 20015, United States; HPCAT, Geophysical Laboratory, Carnegie Institution of Washington, Argonne, Illinois 60439, United States*

Marek Tkacz − *Institute for Physical Chemistry, Polish Academy of Science, 01-224 Warsaw, Poland*

Adam Grzelak − *Centre of New Technologies, University of Warsaw, 02-097 Warsaw, Poland;* orcid.org/0000-0003-4707-3031

Vitali B. Prakapenka − *Consortium for Advanced Radiation Sources, The University of Chicago, Chicago, Illinois 60637, United States;* orcid.org/0000-0001-9270-2330

Complete contact information is available at: https://pubs.acs.org/10.1021/acs.inorgchem.2c00405

Author Contributions

The manuscript was written through contributions of all authors. All authors have given approval to the final version of the manuscript.

Notes

The authors declare no competing financial interest.

■ ACKNOWLEDGMENTS

T.J. thanks the Polish Ministry of Science and Higher education for funding (project "Mobility Plus" no. 1064/MOB/13/2014/0). W.G. acknowledges the Polish National Science Center (NCN) for the Harmonia project 2012/06/M/ST5/00344. T.J. and V.V.S. acknowledge Dr. Ross Hrubiak for the help in the XRD measurements and Dr. Sergey Tkachev for

https://doi.org/10.1021/acs.inorgchem.2c00405
Inorg. Chem. 2022, 61, 8694−8702

Ne loading using the GSECARS gas loading system at the Advanced Photon Source (APS). Use of the COMPRES-GSECARS gas loading system was supported by COMPRES under the National Science Foundation (NSF) Cooperative Agreement EAR 11-57758 and by GSECARS through the NSF grant EAR-1128799 and the DOE grant DE-FG02-94ER14466. Portions of this work were performed at GeoSoilEnviroCARS (The University of Chicago, Sector 13), APS, Argonne National Laboratory. GeoSoilEnviroCARS is supported by NSF − Earth Sciences (EAR-1128799) and DOE − GeoSciences (DE-FG02-94ER14466). Portions of this work were performed at HPCAT (Sector 16), APS Argonne National Laboratory. HPCAT operations are supported by DOE-NNSA under award no. DE-NA0001974 and DOE-BES under award no. DE-FG02-99ER45775, with partial instrumentation funding by NSF. This research used resources of the APS, a U.S. DOE Office of Science User Facility operated by the Argonne National Laboratory under contract no. DE-AC02-06CH11357.

REFERENCES

(1) Schlapbach, L.; Züttel, A. Hydrogen-Storage Materials for Mobile Applications. *Nature* **2001**, *414*, 353−358.
(2) Grochala, W.; Edwards, P. P. Thermal Decomposition of the Non-Interstitial Hydrides for the Storage and Production of Hydrogen. *Chem. Rev.* **2004**, *104*, 1283−1316.
(3) Bannenberg, L. J.; Heere, M.; Benzidi, H.; Montero, J.; Dematteis, E. M.; Suwarno, S.; Jaroń, T.; Winny, M.; Orłowski, P. A.; Wegner, W.; Starobrat, A.; Fijałkowski, K. J.; Grochala, W.; Qian, Z.; Bonnet, J. P.; Nuta, I.; Lohstroh, W.; Zlotea, C.; Mounkachi, O.; Cuevas, F.; Chatillon, C.; Latroche, M.; Fichtner, M.; Baricco, M.; Hauback, B. C.; El Kharbachi, A. Metal (Boro-) Hydrides for High Energy Density Storage and Relevant Emerging Technologies. *Int. J. Hydrogen Energy* **2020**, *45*, 33687−33730.
(4) Modi, P.; Aguey-Zinsou, K. F. Room Temperature Metal Hydrides for Stationary and Heat Storage Applications: A Review. *Front. Energy Res.* **2021**, *9*, No. 128.
(5) Wang, H.; Li, X.; Gao, G.; Li, Y.; Ma, Y. Hydrogen-Rich Superconductors at High Pressures. *Wiley Interdiscip. Rev.: Comput. Mol. Sci.* **2018**, *8*, No. e1330.
(6) Bi, T.; Zarifi, N.; Terpstra, T.; Zurek, E. The Search for Superconductivity in High Pressure Hydrides. In *Reference Module in Chemistry, Molecular Sciences and Chemical Engineering*; Elsevier, 2019.
(7) Gao, G.; Wang, L.; Li, M.; Zhang, J.; Howie, R. T.; Gregoryanz, E.; Struzhkin, V. V.; Wang, L.; Tse, J. S. Superconducting Binary Hydrides: Theoretical Predictions and Experimental Progresses. *Mater. Today Phys.* **2021**, *21*, No. 100546.
(8) Struzhkin, V.; Li, B.; Ji, C.; Chen, X. J.; Prakapenka, V.; Greenberg, E.; Troyan, I.; Gavriliuk, A.; Mao, H. K. Superconductivity in La and Y Hydrides: Remaining Questions to Experiment and Theory. *Matter Radiat. Extremes* **2020**, *5*, No. 028201.
(9) Ashcroft, N. W. Hydrogen Dominant Metallic Alloys: High Temperature Superconductors? *Phys. Rev. Lett.* **2004**, *92*, No. 187002.
(10) Hilleke, K. P.; Zurek, E. Tuning Chemical Precompression: Theoretical Design and Crystal Chemistry of Novel Hydrides in the Quest for Warm and Light Superconductivity at Ambient Pressures. *J. Appl. Phys.* **2022**, *131*, No. 070901.
(11) Li, Y.; Hao, J.; Liu, H.; Li, Y.; Ma, Y. The Metallization and Superconductivity of Dense Hydrogen Sulfide. *J. Chem. Phys.* **2014**, *140*, No. 174712.
(12) Duan, D.; Liu, Y.; Tian, F.; Li, D.; Huang, X.; Zhao, Z.; Yu, H.; Liu, B.; Tian, W.; Cui, T. Pressure-Induced Metallization of Dense (H 2 S) 2 H 2 with High-T c Superconductivity. *Sci. Rep.* **2015**, *4*, No. 6968.
(13) Peng, F.; Sun, Y.; Pickard, C. J.; Needs, R. J.; Wu, Q.; Ma, Y. Hydrogen Clathrate Structures in Rare Earth Hydrides at High Pressures: Possible Route to Room-Temperature Superconductivity. *Phys. Rev. Lett.* **2017**, *119*, No. 107001.
(14) Liu, H.; Naumov, I. I.; Hoffmann, R.; Ashcroft, N. W.; Hemley, R. J. Potential High-Tc Superconducting Lanthanum and Yttrium Hydrides at High Pressure. *Proc. Natl. Acad. Sci. U.S.A.* **2017**, *114*, 6990−6995.
(15) Drozdov, A. P.; Eremets, M. I.; Troyan, I. A.; Ksenofontov, V.; Shylin, S. I. Conventional Superconductivity at 203 Kelvin at High Pressures in the Sulfur Hydride System. *Nature* **2015**, *525*, 73−76.
(16) Geballe, Z. M.; Liu, H.; Mishra, A. K.; Ahart, M.; Somayazulu, M.; Meng, Y.; Baldini, M.; Hemley, R. J. Synthesis and Stability of Lanthanum Superhydrides. *Angew. Chem., Int. Ed.* **2018**, *57*, 688−692.
(17) Somayazulu, M.; Ahart, M.; Mishra, A. K.; Geballe, Z. M.; Baldini, M.; Meng, Y.; Struzhkin, V. V.; Hemley, R. J. Evidence for Superconductivity above 260 K in Lanthanum Superhydride at Megabar Pressures. *Phys. Rev. Lett.* **2019**, *122*, No. 027001.
(18) Drozdov, A. P.; Kong, P. P.; Minkov, V. S.; Besedin, S. P.; Kuzovnikov, M. A.; Mozaffari, S.; Balicas, L.; Balakirev, F. F.; Graf, D. E.; Prakapenka, V. B.; Greenberg, E.; Knyazev, D. A.; Tkacz, M.; Eremets, M. I. Superconductivity at 250 K in Lanthanum Hydride under High Pressures. *Nature* **2019**, *569*, 528−531.
(19) Snider, E.; Dasenbrock-Gammon, N.; McBride, R.; Debessai, M.; Vindana, H.; Vencatasamy, K.; Lawler, K. V.; Salamat, A.; Dias, R. P. Room-Temperature Superconductivity in a Carbonaceous Sulfur Hydride. *Nature* **2020**, *586*, 373−377.
(20) Troyan, I. A.; Semenok, D. V.; Kvashnin, A. G.; Sadakov, A. V.; Sobolevskiy, O. A.; Pudalov, V. M.; Ivanova, A. G.; Prakapenka, V. B.; Greenberg, E.; Gavriliuk, A. G.; Lyubutin, I. S.; Struzhkin, V. V.; Bergara, A.; Errea, I.; Bianco, R.; Calandra, M.; Mauri, F.; Monacelli, L.; Akashi, R.; Oganov, A. R. Anomalous High-Temperature Superconductivity in YH6. *Adv. Mater.* **2021**, *33*, No. 2006832.
(21) Kong, P.; Minkov, V. S.; Kuzovnikov, M. A.; Drozdov, A. P.; Besedin, S. P.; Mozaffari, S.; Balicas, L.; Balakirev, F. F.; Prakapenka, V. B.; Chariton, S.; Knyazev, D. A.; Greenberg, E.; Eremets, M. I. Superconductivity up to 243 K in the Yttrium-Hydrogen System under High Pressure. *Nat. Commun.* **2021**, *12*, No. 5075.
(22) Snider, E.; Dasenbrock-Gammon, N.; McBride, R.; Wang, X.; Meyers, N.; Lawler, K. V.; Zurek, E.; Salamat, A.; Dias, R. P. Synthesis of Yttrium Superhydride Superconductor with a Transition Temperature up to 262 K by Catalytic Hydrogenation at High Pressures. *Phys. Rev. Lett.* **2021**, *126*, No. 117003.
(23) Zurek, E.; Bi, T. High-Temperature Superconductivity in Alkaline and Rare Earth Polyhydrides at High Pressure: A Theoretical Perspective. *J. Chem. Phys.* **2019**, *150*, No. 050901.
(24) Chen, W.; Semenok, D. V.; Huang, X.; Shu, H.; Li, X.; Duan, D.; Cui, T.; Oganov, A. R. High-Temperature Superconducting Phases in Cerium Superhydride with a Tc up to 115 K below a Pressure of 1 Megabar. *Phys. Rev. Lett.* **2021**, *127*, No. 117001.
(25) Di Cataldo, S.; Heil, C.; von der Linden, W.; Boeri, L. LaBH8: Towards High- Low-Pressure Superconductivity in Ternary Superhydrides. *Phys. Rev. B* **2021**, *104*, No. L020511.
(26) Hirano, K.; Kadono, J.; Yamamoto, S.; Tanabe, T.; Miyake, H. Hydrogen-Absorbing Characteristics of 15 Rare Earth Elements. *J. Alloys Compd.* **2006**, *408*−*412*, 351−354.
(27) Matsuoka, T.; Fujihisa, H.; Hirao, N.; Ohishi, Y.; Mitsui, T.; Masuda, R.; Seto, M.; Yoda, Y.; Shimizu, K.; MacHida, A.; Aoki, K. Structural and Valence Changes of Europium Hydride Induced by Application of High-Pressure H2. *Phys. Rev. Lett.* **2011**, *107*, No. 025501.
(28) Kuno, K.; Matsuoka, T.; Masuda, R.; Mitsui, T.; Seto, M.; Machida, A.; Fujihisa, H.; Hirao, N.; Ohishi, Y.; Shimizu, K.; Sasaki, S. Mixed-Valence State and Structure Changes of EuHx (X = 2 and $2 < x \leq 3$) under High-Pressure H2 Atmosphere. *J. Alloys Compd.* **2021**, *865*, No. 158637.
(29) Semenok, D. V.; Zhou, D.; Kvashnin, A. G.; Huang, X.; Galasso, M.; Kruglov, I. A.; Ivanova, A. G.; Gavriliuk, A. G.; Chen, W.; Tkachenko, N. V.; Boldyrev, A. I.; Troyan, I.; Oganov, A. R.; Cui, T. Novel Strongly Correlated Europium Superhydrides. *J. Phys. Chem. Lett.* **2021**, *12*, 32−40.

https://doi.org/10.1021/acs.inorgchem.2c00405
Inorg. Chem. 2022, 61, 8694−8702

(30) Warf, J. C.; Hardcastle, K. A Higher Hydride Of Ytterbium. *J. Am. Chem. Soc.* **1961**, *83*, 2206−2207.
(31) Warf, J. C.; Hardcastle, K. I. Rare Earth-Hydrogen Systems. IV. The Higher Hydride of Ytterbium, a New Type of Hydride. *Inorg. Chem.* **1966**, *5*, 1736−1740.
(32) Iwasieczko, W.; Drulis, M.; Drulis, H. Magnetic Properties of the *β*- and B′-Ytterbium Hydride Phases. *J. Alloys Compd.* **2001**, *327*, 11−16.
(33) Auffermann, G. Hochdrucksynthese Und Kristallstruktur von YbH2,67. *Z. Anorg. Allg. Chem.* **2002**, *628*, 1615−1618.
(34) Jaroń, T.; Grochala, W.; Hoffmann, R. Towards Superconductivity in Hydrides: Computational Studies of Two Hypothetical Ternary Compounds, YbIIBeH4 and Cs3YbIIIH6. *J. Mol. Model.* **2007**, *13*, 769−774.
(35) Li, Y.; Hao, J.; Liu, H.; Tse, J. S.; Wang, Y.; Ma, Y. Pressure-Stabilized Superconductive Yttrium Hydrides. *Sci. Rep.* **2015**, *5*, No. 9948.
(36) Sun, W.; Kuang, X.; Keen, H. D. J.; Lu, C.; Hermann, A. Second Group of High-Pressure High-Temperature Lanthanide Polyhydride Superconductors. *Phys. Rev. B* **2020**, *102*, No. 144524.
(37) Jaron, T.; Ying, J.; Tkacz, M.; Grzelak, A.; Prakapenka, V. B.; Struzhkin, V. V.; Grochala, W. Synthesis, Structure and Electric Conductivity of Higher Hydrides of Ytterbium at High Pressure. 2022.
(38) Rivers, M.; Prakapenka, V.; Kubo, A.; Pullins, C.; Holl, C.; Jacobsen, S. The COMPRES/GSECARS Gas-Loading System for Diamond Anvil Cells at the Advanced Photon Source. *High Pressure Res.* **2008**, *28*, 273−292.
(39) Prakapenka, V. B.; Kubo, A.; Kuznetsov, A.; Laskin, A.; Shkurikhin, O.; Dera, P.; Rivers, M. L.; Sutton, S. R. Advanced Flat Top Laser Heating System for High Pressure Research at GSECARS: Application to the Melting Behavior of Germanium. *High Pressure Res.* **2008**, *28*, 225−235.
(40) Prescher, C.; Prakapenka, V. B. DIOPTAS: A Program for Reduction of Two-Dimensional X-Ray Diffraction Data and Data Exploration. *High Pressure Res.* **2015**, *35*, 223−230.
(41) Neumann, M. A. X-Cell: A Novel Indexing Algorithm for Routine Tasks and Difficult Cases. *J. Appl. Crystallogr.* **2003**, *36*, 356−365.
(42) Petricek, V.; Dusek, M.; Palatinus, L.; Petříček, V.; Dušek, M.; Palatinus, L.; Petrícek, V.; Dušek, M.; Palatinus, L. Crystallographic Computing System JANA2006: General Features. *Z. Kristallogr. - Cryst. Mater.* **2014**, *229*, 345−352.
(43) Angel, R. J.; Gonzalez-Platas, J.; Alvaro, M. EosFit7c and a Fortran Module (Library) for Equation of State Calculations. *Z. Kristallogr. - Cryst. Mater.* **2014**, *229*, 405−419.
(44) Gonzalez-Platas, J.; Alvaro, M.; Nestola, F.; Angel, R. EosFit7-GUI: A New Graphical User Interface for Equation of State Calculations, Analyses and Teaching. *J. Appl. Crystallogr.* **2016**, *49*, 1377−1382.
(45) Clark, S. J.; Segall, M. D.; Pickard, C. J.; Hasnip, P. J.; Probert, M. I. J. J.; Refson, K.; Payne, M. C. First Principles Methods Using CASTEP. *Z. Kristallogr. - Cryst. Mater.* **2005**, *220*, 567−570.
(46) Perdew, J. P.; Ruzsinszky, A.; Csonka, G. I.; Vydrov, O. A.; Scuseria, G. E.; Constantin, L. A.; Zhou, X.; Burke, K. Restoring the Density-Gradient Expansion for Exchange in Solids and Surfaces. *Phys. Rev. Lett.* **2008**, *100*, No. 136406.
(47) Takemura, K.; Syassen, K. Pressure-Volume Relations and Polymorphism of Europium and Ytterbium to 30 GPa. *J. Phys. F Met. Phys.* **1985**, *15*, 543−559.
(48) Olsen, J. S.; Buras, B.; Gerward, L.; Johansson, B.; Lebech, B.; Skriver, H. L.; Steenstrup, S. A New High-Pressure Phase and the Equation of State of YbH2. *Phys. Scr.* **1984**, *29*, 503−507.
(49) Klotz, S.; Casula, M.; Komatsu, K.; Machida, S.; Hattori, T. High-Pressure Structure and Electronic Properties of YbD2 to 34 GPa. *Phys. Rev. B* **2019**, *100*, No. 020101.
(50) Salke, N. P.; Davari Esfahani, M. M.; Yedukondalu, N.; Zhang, Y.; Kruglov, I. A.; Zhou, J.; Greenberg, E.; Prakapenka, V. B.; Liu, J.; Oganov, A. R.; Lin, J. F. Prediction and Synthesis of Dysprosium Hydride Phases at High Pressure. *Inorg. Chem.* **2020**, *59*, 5303−5312.
(51) Palasyuk, T.; Tkacz, M. Pressure-Induced Structural Phase Transition in Rare-Earth Trihydrides. Part II. SmH3 and Compressibility Systematics. *Solid State Commun.* **2007**, *141*, 302−305.
(52) Manjón, F.; Tresserras, J. A. S.; Ibáñez, J.; Pereira, A. L. J. Pressure-Induced Phase Transitions in Sesquioxides. *Crystals* **2019**, *9*, 630.
(53) Grochala, W.; Hoffmann, R.; Feng, J.; Ashcroft, N. W. The Chemical Imagination at Work InVery Tight Places. *Angew. Chem., Int. Ed.* **2007**, *46*, 3620−3642.
(54) Matsuoka, T.; Fujihisa, H.; Hirao, N.; Ohishi, Y.; Mitsui, T.; Masuda, R.; Seto, M.; Yoda, Y.; Shimizu, K.; Machida, A.; Aoki, K. Erratum: Structural and Valence Changes of Europium Hydride Induced by Application of High-Pressure H2 (Physical Review Letters (2011) 107 (025501) DOI: 10.1103/PhysRevLett.107.025501). *Phys. Rev. Lett.* **2019**, *122*, No. 179901.
(55) Olsen, J. E.; Frommen, C.; Sørby, M. H.; Hauback, B. C. Crystal Structures and Properties of Solvent-Free LiYb(BH4)4−xClx, Yb(BH4)3 and Yb(BH4)2−xClx. *RSC Adv.* **2013**, *3*, 10764−10774.
(56) Eirik Olsen, J.; Frommen, C.; Jensen, T. R.; Riktor, M. D.; Sørby, M. H.; Hauback, B. C. Structure and Thermal Properties of Composites with RE-Borohydrides (RE= La, Ce, Pr, Nd, Sm, Eu, Gd, Tb, Er, Yb or Lu). *RSC Adv.* **2014**, *4*, 1570−1582.
(57) Wegner, W.; Jaroń, T.; Grochala, W. Preparation of a Series of Lanthanide Borohydrides and Their Thermal Decomposition to Refractory Lanthanide Borides. *J. Alloys Compd.* **2018**, *744*, 57−63.
(58) Wegner, W.; Jaroń, T.; Grochala, W. MYb(BH4)4 (M = K, Na) from Laboratory X-Ray Powder Data. *Acta Crystallogr., Sect. C: Cryst. Struct. Commun.* **2013**, *69*, 1289−1291.
(59) Chen, K.; Baudelet, F.; Mijiti, Y.; Nataf, L.; Di Cicco, A.; Hu, Z.; Agrestini, S.; Komarek, A. C.; Sougrati, M.; Haines, J.; Rouquette, J.; Kong, Q.; Weng, T. C. Revisiting the Phase Transition of Magnetite under Pressure. *J. Phys. Chem. C* **2019**, *123*, 21114−21119.
(60) Liu, L. L.; Sun, H. J.; Wang, C. Z.; Lu, W. C. High-Pressure Structures of Yttrium Hydrides. *J. Phys. Condens. Matter* **2017**, *29*, No. 325401.

https://doi.org/10.1021/acs.inorgchem.2c00405
Inorg. Chem. 2022, 61, 8694−8702